Physica D 239 (2010) 757–765

Contents lists available at ScienceDirect

Physica D

journal homepage: www.elsevier.com/locate/physd

Front propagation in the bromate–sulfite–ferrocyanide–aluminum (III) system: Autocatalytic front in a buffer system

Klara Kovacs, Marcin Leda, Vladimir K. Vanag, Irving R. Epstein *

Department of Chemistry, Brandeis University, MS 015, Waltham, MA 02454, USA

ARTICLE INFO

Article history:
Available online 18 June 2009

Keywords:
Front propagation
Buffer
pH oscillator

ABSTRACT

We study the propagation of pH fronts in a narrow, pseudo-one-dimensional strip of gel containing bromate, sulfite, ferrocyanide and aluminum ions. The front propagation speed v decreases with $[Al^{3+}]$ as $1/v = 1/v_0 + c[Al^{3+}]$, where c is a constant. We determine the diffusion coefficients of protons and ferricyanide ions and find that $Al(OH)_3$ loaded in agarose or acrylamide gels binds protons reversibly, thereby slowing the propagating fronts without significantly affecting the diffusion of ferricyanide ions. We present a model that qualitatively reproduces the experimental behavior, and we suggest some general principles governing autocatalytic fronts in buffered systems.

1. Introduction

Since the first discovery of dissipative patterns in the ferrocyanide–iodate–sulfite reaction [1] (FIS system) almost 15 years ago [1–4], many attempts to reproduce these experiments in other laboratories have been unsuccessful. Very recently, stationary labyrinthine patterns in the FIS system have again been generated [5]. Szalai and De Kepper [5] emphasize that their success is based on the introduction of a charged polymer, poly(acrylate) (PA), into the inert agarose gel. This polymer possesses carboxylic side groups, COO^-, that reversibly bind protons, thereby decreasing the effective diffusion coefficient of H^+. Although this very plausible idea still requires experimental verification, it raises a question about the role of "buffers" in pattern formation and in front propagation in particular. If we look carefully at two of the most extensively studied pattern-forming chemical systems, the chlorine dioxide-iodide-malonic acid (CDIMA) and the Belousov–Zhabotinsky-AOT (BZ-AOT) systems, we observe that a "buffer" with small diffusivity is present in each of those systems. In the CDIMA reaction, the role of the buffer is played by large starch (or poly(vinyl alcohol)) molecules that reversibly bind I_3^-, where I^- (part of which is complexed as I_3^-) is the key activator species in this reaction. In the BZ-AOT system, a monolayer shell of the surfactant AOT (sodium bis(2-ethylhexyl) sulfosuccinate) surrounds the water nano-droplets in which the reaction takes place. The AOT shell reversibly sequesters a large amount of Br_2 (a key species that plays the role of a fast-diffusing inhibitor), thus reducing the effective diffusion coefficient of Br_2 in the oil phase. The related problem of diffusion of Ca^{2+} ions in a cell with mobile and immobile buffers has been treated by Wagner and Keizer [6].

In experiments analogous to those on the FIS system, we have recently observed (unpublished result) quasi-stationary spots in another pH oscillator, the BrO_3^-–SO_3^{2-}–$Fe(CN)_6^{4-}$–$Al(OH)_3$ (BSFA) reaction, in a one-sided CFUR (continuously fed unstirred reactor). This system is composed of the well-known bromate–sulfite–ferrocyanide (BSF) [7] oscillatory reaction coupled to the $Al(OH)_3$ precipitation equilibrium [8,9]. We suggest that these patterns arise as the result of reversible coupling of free protons to large particles of precipitated $Al(OH)_3$. Thus, in both the FIS and the BSFA system, coupling between H^+ and large particles, which act as a buffer, can lead to dissipative patterns.

In this work, we examine this idea further by investigating the velocity of front propagation in a gel loaded with the components of the BSFA system, as well as by measuring the diffusion coefficients of key components of the BSFA system in a gel in the presence and absence of $Al(OH)_3$ precipitate. We also carry out a theoretical investigation of this problem, both analytically and numerically. We note that patterns in the bromate–sulfite reaction have been studied in a CFUR [10], and front propagation in the bromate–sulfite reaction in an aqueous system without gel was investigated in order to examine the effect of convection on front propagation [11].

2. Experimental and results

The front velocity was measured in a long, narrow slice of gel (polyacrylamide or agarose) sandwiched between two flat glass plates as described elsewhere [12] and shown in Fig. 1a. The gel was first immersed in an aluminum nitrate solution for 15 min. Next, we added the sulfite and the indicator solution

* Corresponding address: Department of Chemistry, Brandeis University, 415 South Street, MS 015, Waltham, MA, 02454, USA. Tel.: +1 781 736 2503.
E-mail address: epstein@brandeis.edu (I.R. Epstein).

0167-2789/$ – see front matter © 2009 Elsevier B.V. All rights reserved.
doi:10.1016/j.physd.2009.06.006

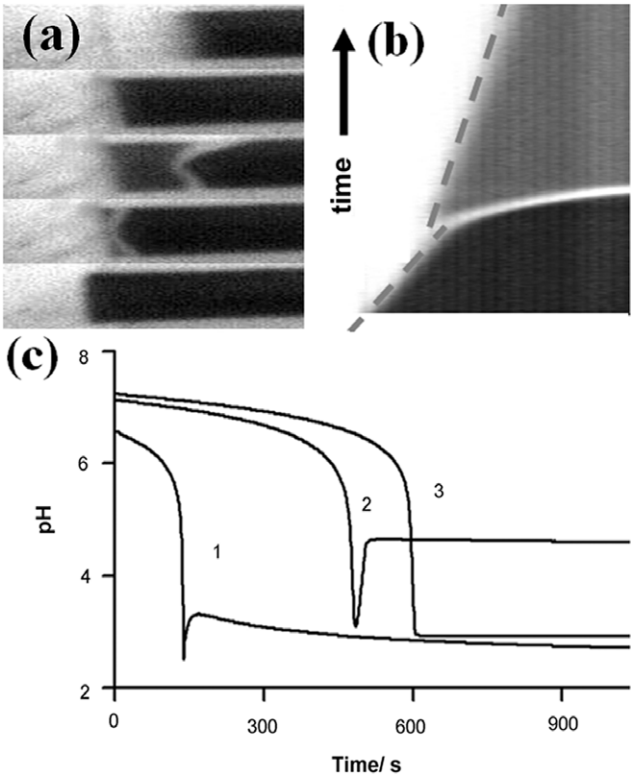

Fig. 1. (a) Snapshots of a polyacrylamide gel slice with a propagating pH front, taken at (from bottom to top): 0, 220, 300, 360, and 1520 s. (b) Space–time plot (4.15 mm × 680 s) made along the long axis of the gel (0.3 mm thick) at $[Fe(CN)_6^{4-}]_0 = 0.015$ M, $[SO_3^{2-}]_0 = 0.075$ M, $[H^+]_0 = 0.02$ M, $[BrO_3^-]_0 = 0.065$ M, $[Al^{3+}]_0 = 0.01$ M, [Bromophenol blue] $= 1.1 \times 10^{-3}$ M. Dotted lines show the slopes from which the front velocities were measured. (c) Autocatalytic reactions in a stirred tank reactor at $[Fe(CN)_6^{4-}]_0 = 0.015$ M, $[SO_3^{2-}]_0 = 0.075$ M, $[BrO_3^-]_0 = 0.065$ M, $[Al^{3+}]_0$/M = (curves 1 and 2) 0.01, (3) 0; $[H^+]_0 =$ (curves 1 and 3) 0.02 M and the initial pH is adjusted to 7.15 (by adding 0.1 M NaOH) in curve 2.

and waited for 5 min. Finally, since the induction time of the reaction is between 7 and 10 min, depending on initial conditions, we immersed the gel in a solution containing the remaining components of the BSFA system for 2 min. As a result of this procedure, the initial concentrations of bromate and ferrocyanide in the gel may be slightly less than in the solution, but keeping the time of immersion constant gives the same initial concentrations of BrO_3^- and $Fe(CN)_6^{4-}$ for different experiments. The initial pH was approximately 7.

We then initiated the front by switching one end of the gel to pH 3 by touching it with another piece of a gel prepared at the lower pH. The front converts the system from an unstable state at pH 7 to a stable steady state (SS) at low pH (the final pH depends on the concentration of $Fe(CN)_6^{4-}$ and can vary between 2 and 4.3). We followed the front propagation with a CCD camera either at wavelength 410 nm, which corresponds to the absorption of ferricyanide, or, with added pH indicator, bromophenol blue, at 600 nm (the indicator changes from blue at pH $>$ 4.6 to yellow at pH $<$ 3). If we follow the reaction using the absorption of ferricyanide, we observe only one simple front similar to a typical Fisher–Kolmogorov (FK) front that links the stable and unstable SSs. If we use the pH indicator, we can see two fronts as shown in Fig. 1a. The first is the same as the front seen by monitoring ferricyanide, and both methods of observation gave the same velocity under the same set of conditions. The second front emerges after the global autocatalytic reaction transforms the entire gel stripe: the gel suddenly turns yellow, and behind this fast autocatalytic front the gel turns blue again. This phenomenon causes the observed wavy stripes in Fig. 1a. The second front can be observed only using a pH indicator and cannot be seen by following the ferricyanide concentration changes in the absence of added indicator. We therefore conclude that these changes involve only the H^+ concentration. On the other hand, the second front does not appear without ferrocyanide. Note also that increasing the initial ferrocyanide concentration decreases the front rate and increases the induction period of the autocatalytic reaction. The last circumstance is convenient, since it allows more time to observe front propagation before global autocatalysis begins.

A typical space–time plot for front propagation is shown in Fig. 1b. The velocities of the two fronts were obtained as the slopes of this plot. The slope of the dashed line separating the white and black regions during the first few minutes gives us the velocity of the first front. Then there is a transition from the high to the low pH state in the entire gel (the nearly horizontal white line in Fig. 1b). This transition is followed almost immediately by a rebound in the pH, which can be observed in the color change of the indicator (gray region in the space–time plot, which implies that the pH must be above 4.6). After this pH rebound, a second, much slower front returns the system to the stable SS at smaller pH. The velocity of this front corresponds to the slope of the dashed line separating the white and gray regions. In the BSF system without Al^{3+}, we see only a single front, and the system simply goes from the unstable high pH initial state to the stable low pH SS, as in the lower portion of Fig. 1b.

To try to understand the behavior of the fronts, we ran the reaction under similar conditions in a stirred closed reactor. Fig. 1c shows the resulting pH–time curves. In the absence of added Al^{3+} (curve 3) there is a single sharp transition between the initial and final states, in good agreement with the simple front observed in the BSF system. Curves 1 and 2 show the pH changes when $Al(NO_3)_3$ is present. The initial pH of curve 2 was adjusted to about 7 to more closely mimic the experimental conditions in the gel. Even without adjusting the initial pH (curve 1), it is clear that the pH changes much more rapidly in the presence of $[Al^{3+}]_0$. In both of the curves with added Al^{3+} we observe a sudden increase of the pH after the initial fast autocatalytic reaction between bromate and sulfite. This rise corresponds to the fast pH increase when the indicator turns blue again in the gel experiments. Then, at sufficiently high $[Al^{3+}]_0$, the pH decreases slowly for about an hour until it reaches pH $\sim$ 3, corresponding to the slow second front; after that it rises again and after 3 h stabilizes at pH = 4.3. If $[Al^{3+}]_0 \leq 0.006$ M, the system stabilizes between pH 2 and 3.

The first front, which depends on the autocatalytic reaction between sulfite and bromate, is similar to a Fisher–Kolmogorov front, though the initial high pH state in our case is not the true steady state, which coincides with an unreachable zero concentration of protons. Therefore its behavior is more generic, and we focus our efforts (both experimental and theoretical) on this first front. The dependence of the velocity of this front on $[Al^{3+}]_0$ in polyacrylamide gel is shown in Fig. 2. The front propagation speed decreases with the initial aluminum concentration and can be approximated as $1/v = 1/v_0 + c[Al^{3+}]_0$, where $c \cong 268$ min/(mm × M), $[Al^{3+}]_0$ is the total concentration of added Al-ions, and v_0 is the front velocity in the corresponding BSF system (without aluminum). We observe a similar dependence of v on $[Al^{3+}]_0$ in agarose gel. The velocity of the second front also decreases with $[Al^{3+}]_0$.

It is well known [13] that the velocity v of a Fisher–Kolmogorov front depends on the autocatalytic rate, k, and the diffusion coefficient of the activator (H^+ in our case), D_h, as $2(kD_h)^{1/2}$. In Fig. 1c, we see that the rate of autocatalysis does not diminish in the presence of $Al(OH)_3$. Therefore the decrease in v with $Al(OH)_3$ can be explained by the decrease in the effective diffusion coefficient D_h. To test this idea, we carried out measurements of

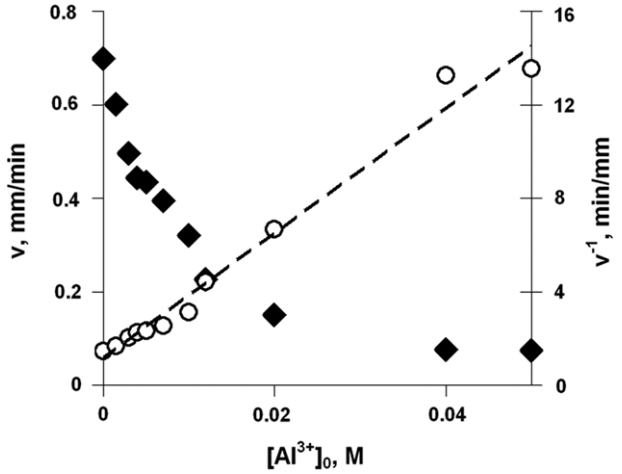

Fig. 2. Dependence of front velocity in the BSFA system on Al^{3+} in polyacrylamide gel at $[Fe(CN)_6^{4-}]_0 = 0.015$ M, $[SO_3^{2-}]_0 = 0.075$ M, $[H^+]_0 = 0.02$ M, and $[BrO_3^-]_0 = 0.065$ M. Rhombs, v; open circles, v^{-1}.

diffusion coefficients in a glass gel holder. The glass surface was made hydrophobic with (tridecafluoro-1,1,2,2-tetrahydrooctyl) trichlorosilane. The gel layer was 1 mm thick and 10 mm wide. A layer of solution injected next to the gel had the same volume as the gel. We followed the diffusion of ferricyanide and of protons with a CCD camera. Space–time plots of these measurements have a parabolic shape (Fig. 3a). We obtained the relative diffusion constants by plotting the square of the front position *vs.* time and using the relationship $\langle x^2 \rangle = 2c_p Dt$, where x is the mean displacement (front position), D is the diffusion coefficient, t is the time, and c_p is a constant of order 1 that depends on the exact "position" of the front and can be larger or smaller than unity depending on the $[H^+]$ chosen to specify that position. We do not know c_p, since we do not know the relationship between $[H^+]$ and the gray levels in Fig. 3a. Therefore our measurements of D_h are accurate only in a relative sense.

The diffusion coefficient of ferricyanide D_F did not change significantly with the concentration of $Al(OH)_3$ in the gel (Fig. 3b). The small increase in D_F seen in Fig. 3b is within our experimental error (10%–20%). On the other hand, the effective diffusion coefficient of H^+ decreased with $[Al(OH)_3]$. In both acrylamide and agarose gels, addition of 0.01 M Al^{3+} decreased the diffusion rate of protons by a factor of 6 to 7.

3. Theoretical analysis

To get more insight into the front propagation observed in our rather complex system, we can abstract the key features and represent them by simple models, which we examine in detail. We note that there are two different sets of protonation reactions that can affect the speed of the front. These are the autocatalytic protonation of the sulfite substrate, which can be found in three different forms: H_2SO_3, HSO_3^-, and SO_3^{2-} and the protonation of the precipitate $Al(OH)_3$ to form $Al(OH)_2^+$ and $Al(OH)^{2+}$ We start by considering these protonation reactions separately and in a simpler form, taking into account only two forms for the substrate and two for the precipitate. Later, we will look at more complex systems.

System I. Our first model system is

$$s + h \to 2h \quad k_1, (M^{-1}s^{-1}) \tag{1}$$

$$p_0 + h \rightleftarrows p_1 \quad K_P, (M^{-1}) \tag{2}$$

where

$$p_0 + p_1 = p. \tag{3}$$

Reaction 1 is autocatalysis with substrate s and protons h; it is a caricature of the sulfite subsystem in the BSF or BSFA reaction and is a general feature of many pH oscillators. The species P (with concentration p) can exist in either of two forms: deprotonated p_0 and protonated p_1. P can be identified with the large polymer molecules added to the FIS system [5]. In our BSFA system, P_0 may represent either the $Al(OH)_3$ precipitate or the small molecule $Al(OH)_2^-$ (with $Al(OH)^{2-}$ as P_1). If P_0 is $Al(OH)_3$, reaction 2 may exhibit more complex kinetics, a case we consider below.

Note that in a stirred system or in a spatially extended system with $D_P = 0$ (e.g., if P is a large molecule), p is constant in space, while in a spatially extended system with $D_P \neq 0$, even with an initially uniform distribution of p, gradients of p can arise as a result of the front propagation. System (1), (2) can be described by the partial differential equations

$$\partial h/\partial t = k_1 sh + R_P + D_h \nabla^2 h \tag{4}$$

$$\partial s/\partial t = -k_1 sh + D_S \nabla^2 s \tag{5}$$

$$\partial p_0/\partial t = R_P + D_P \nabla^2 p_0 \tag{6}$$

$$\partial p_1/\partial t = -R_P + D_P \nabla^2 p_1 \tag{7}$$

where $R_P = -k_d p_0 h + (k_d/K_P) p_1$, and k_d is the diffusion-controlled association rate constant (typical for protonation reactions). D_h, D_S, and D_P are the corresponding diffusion coefficients, where we have made the approximation that p_0 and p_1 have the same value, D_P, $\nabla = \partial/\partial x$, and x is the spatial coordinate. Following [6], we seek to eliminate the fast equilibrium reaction term R_P. We write down the identity:

$$h + p_1 = h + pE_P \tag{8}$$

where $p_1 = pE_P$ and, assuming that the equilibrium in Eq. (2) is rapidly established,

$$E_P = K_P h/(1 + K_P h). \tag{9}$$

Differentiation of Eq. (8) with respect to time gives

$$\partial h/\partial t + \partial p_1/\partial t = W_1 \partial h/\partial t + (\partial p/\partial t) E_P \tag{10}$$

where

$$W_1 \equiv 1 + pG_P \tag{11}$$

$$G_P \equiv \mathrm{d}E_P/\mathrm{d}h = K_P/(1 + K_P h)^2. \tag{12}$$

Substituting Eqs. (4) and (7) into the left-hand side of Eq. (10), we have

$$k_1 sh + D_h \nabla^2 h + D_P \nabla^2 (pE_P) = W_1 \partial h/\partial t + (\partial p/\partial t) E_P. \tag{13}$$

Combining Eqs. (6) and (7) we find

$$\partial p/\partial t = D_P \nabla^2 p. \tag{14}$$

An analogous, but more cumbersome, procedure can be carried out if we allow different D_P for p_0 and p_1. Substituting Eq. (14) into Eq. (13), we have:

$$W_1 \partial h/\partial t = k_1 sh + D_h \nabla^2 h + D_P \nabla^2 (pE_P) - E_P D_P \nabla^2 p. \tag{15}$$

Expanding the Laplacian terms, for example,

$$\nabla^2 (pE_P) = E_P \nabla^2 p + 2\nabla p \bullet \nabla E_P + p\nabla^2 E_P \tag{16}$$

("•" is the scalar product of two vectors), Eq. (15) becomes

$$W_1 \partial h/\partial t = k_1 sh + D_h \nabla^2 h + 2D_P \nabla p \bullet \nabla E_P + pD_P \nabla^2 E_P. \tag{17}$$

Note that

$$\nabla E_P = G_P \nabla h \quad \text{and} \quad \nabla^2 E_P = G_P \nabla^2 h + V_P \nabla h \bullet \nabla h \tag{18}$$

where

$$V_P \equiv -2K_P^2/(1 + K_P h)^3 = \mathrm{d}^2 E_P/\mathrm{d}h^2 \tag{19}$$

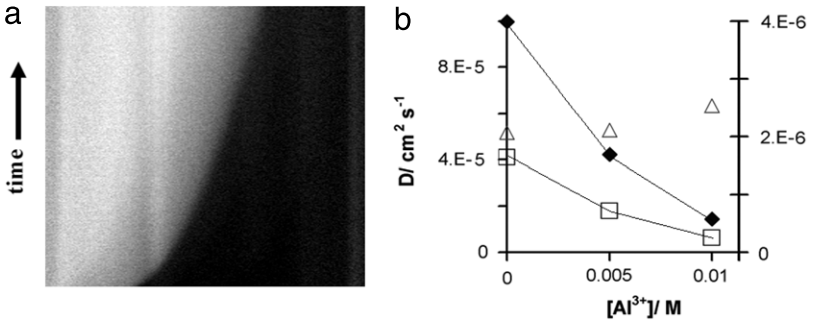

Fig. 3. (a) Typical parabolic space–time plot of an H^+ diffusion measurement. 1.4×10^{-4} M bromophenol blue indicator in the acrylamide gel was used to see the proton diffusion. The space–time plot was made along a 14.69 mm × 3800 s gel slice of 1 mm thickness. (b) Effective diffusion coefficients as a function of Al^{3+}. (Δ) for 0.02 $MK_3[Fe(CN)_6]$ in polyacrylamide gel (right scale); (♦) for 0.01 M HCl in agarose gel and (□) in polyacrylamide gel (left scale). The ionic strength was adjusted with KCl (or NaCl) up to the usually used value 0.12 M.

and Eq. (17) transforms to

$$W_1 \partial h/\partial t = k_1 s h + (D_h + p D_P G_P)\nabla^2 h + p D_P V_P \nabla h \bullet \nabla h + 2 D_P G_P \nabla p \bullet \nabla h. \tag{20}$$

Introducing the effective Fickian diffusion coefficient, D_h^*, as

$$D_h^* = (D_h + p D_P G_P)/W_1. \tag{21}$$

Eq. (20) for $\partial h/\partial t$ assumes the final form

$$\partial h/\partial t = k_1 s h/W_1 + D_h^* \nabla^2 h + H_h \nabla h \bullet \nabla h + H_P \nabla p \bullet \nabla h \tag{22}$$

where

$$H_P = 2 D_P G_P / W_1 \quad \text{and} \quad H_h = p D_P V_P / W_1. \tag{23}$$

Eqs. (5), (14) and (22) constitute our simplest model. If $D_P = 0$, e.g., if P represents solid precipitate particles, Eq. (22) becomes

$$\partial h/\partial t = (k_1 s h + D_h \nabla^2 h)/(1 + p G_P). \tag{24}$$

Thus, the effect of the buffer species P in step (2) is to rescale both the rate of production and the diffusion of protons in step (1) in a pH-dependent fashion governed by the denominator in Eq. (24). An analogous rescaling was obtained for the diffusion of iodide in the CDIMA reaction due to formation of the starch/triiodide complex [14] and for the diffusion of protons in the chlorite–tetrathionate reaction due to protonation of carboxylate groups of the immobile polymer [15].

For the system of Eqs. (5) and (24) with p = constant (since $D_P = 0$), we can introduce a moving frame $r = x - vt$ with velocity v that transforms partial differential equations (5), (24) into the following ordinary differential equations

$$\mathrm{d}h/\mathrm{d}r = g_h \tag{25}$$

$$\mathrm{d}s/\mathrm{d}r = g_S \tag{26}$$

$$\mathrm{d}g_h/\mathrm{d}r = -k_1 s h/D_h - (1 + p G_P) v g_h/D_h \tag{27}$$

$$\mathrm{d}g_S/\mathrm{d}r = k_1 s h/D_S - (v/D_S) g_S. \tag{28}$$

The system (25)–(28) has two steady states, $g_h = g_S = h = 0$, $s = s_{in}$ (SS1) and $g_h = g_S = s = 0$, $h = h_f$ (SS2), where s_{in} is the initial concentration of substrate s, and h_f is the final concentration of h. Of course, SS1 with $h = 0$ is impossible (due to dissociation of water), but we can assume that if an initial state (in experiment) has very small h_0, the resulting experimental front speed will be close to the theoretical one found below. Later we analyze numerically what happens if the initial h_0 is not very small. Analyzing the linear stability of SS1 (SS2 is a saddle point and is not of interest [13]), we can write the following equation for the eigenvalues λ of the corresponding Jacobian matrix for system (25)–(28)

$$\lambda(v/D_S + \lambda)[\lambda^2 + \lambda(1 + pK_P)v/D_h + k_1 s_{in}/D_h] = 0 \tag{29}$$

where we use the fact that $G_P = K_P$ at $h = 0$. The eigenvalues λ must be real, because complex values would result in oscillations around $h = 0$, which would lead to negative values of h. Therefore, the discriminant of the quadratic function in (29) must be positive, which implies that

$$v > v_{\min} = 2(k_1 s_{in} D_h)^{1/2}/(1 + pK_P). \tag{30}$$

The marginal stability principle [16–18] implies that the front velocity for Fisher–Kolmogorov type fronts in this system will tend to $v_{\min}$ and that fronts with $v > v_{\min}$ must decelerate.

We expect that a result analogous to Eq. (30) will persist for small non-zero values of D_P. Direct numerical integration of Eqs. (4)–(7) nicely confirms this result. In our simulations, we found that the front velocity is directly proportional to $k_1^{1/2}$, $D_h^{1/2}$, and almost independent of D_S (at least at $D_S \ll D_h$). To find how v depends on p and K_P, we used values of diffusion coefficients close to those in our experiments: $D_h = 2 \times 10^{-4}$ cm^2 s^{-1}, $D_S = 1 \times 10^{-5}$ cm^2 s^{-1}, $D_P = 1 \times 10^{-7}$ cm^2 s^{-1}; we also fixed $s_{in} = 10^{-3}$ M. We found numerically that $1/v = c_1 p + b$ at constant K_P and $1/v = c_2 K_P + b$ at constant p, where c_1, c_2, and b are constants that can be evaluated from Eq. (30) as

$$b = 1/(4k_1 s_{in} D_h)^{1/2}, \qquad c_1 = K_P/(4k_1 s_{in} D_h)^{1/2}, \quad \text{and} \quad c_2 = p/(4k_1 s_{in} D_h)^{1/2}. \tag{31}$$

The measured wave speeds are larger than those given by Eq. (30), but by no more than 20%–30%. A possible explanation for this small discrepancy is that it takes longer than the time of our experiment for v to reach its final value of $v_{\min}$. As predicted by Eq. (30), our experimental dependence of $1/v$ on $[Al^{3+}]_0$ is linear (Fig. 2). The equilibrium constant K_P for protonation of the precipitate in the gel can be obtained as the ratio of the slope of this plot (c_1) to the value of the intercept b.

Subsystem II. Two protonated forms of substrate. Consider now the following system

$$s_1 + h \to 2h, \quad k_1, \tag{32}$$

$$s_0 + h \rightleftarrows s_1, \quad K_S \tag{33}$$

where

$$s_0 + s_1 = s \tag{34}$$

$$s_1 = s E_S \tag{35}$$

$$E_S = K_S h/(1 + K_S h). \tag{36}$$

The corresponding partial differential equations are

$$\partial h/\partial t = k_1 s_1 h + R_S + D_h \nabla^2 h \tag{37}$$

$$\partial s_1/\partial t = -k_1 s_1 h - R_S + D_S \nabla^2 s_1 \tag{38}$$

$$\partial s_0/\partial t = R_S + D_S \nabla^2 s_0 \tag{39}$$

where D_S is the same for s_0 and s_1, $R_S = -k_d s_0 h + (k_d/K_S)s_1$, and k_d is the association rate constant. As before, we start from the identity

$$h + s_1 = h + sE_S. \tag{40}$$

Differentiation with respect to time gives

$$\partial h/\partial t + \partial s_1/\partial t = W_2 \partial h/\partial t + (\partial s/\partial t)E_S \tag{41}$$

where

$$W_2 = 1 + sG_S, \quad G_S = \partial E_S/\partial t = K_S/(1 + K_S h)^2. \tag{42}$$

Following the same procedure as above, we finally obtain

$$\partial h/\partial t = k_1 s h E_S^2/W_2 + D_h' \nabla^2 h + H_S \nabla s \bullet \nabla h + H_h \nabla h \bullet \nabla h \tag{43}$$

$$\partial s/\partial t = -k_1 s E_S h + D_S \nabla^2 s \tag{44}$$

where

$$\begin{aligned} &D_h' = (D_h + D_S s G_S)/W_2, \qquad H_S = 2D_S G_S/W_2, \\ &H_h = sD_S V_S/W_2, \qquad V_S \equiv E_S'' = -2K_S^2/(1 + K_S h)^3. \end{aligned} \tag{45}$$

Numerical simulations show that if $D_S \ll D_h$, then the front velocity is almost independent of D_S, and we can put $D_S = 0$. In this case, Eqs. (43) and (44) are considerably simplified, and their analytical solution can be found. With $D_S = 0$ Eqs. (43) and (44) become

$$\partial h/\partial t = (k_1 s h E_S^2 + D_h \nabla^2 h)/W_2 \tag{46}$$

$$\partial s/\partial t = -k_1 s E_S h. \tag{47}$$

Unlike the models analyzed above, Eqs. (43) and (44), (or Eqs. (46) and (47)) do not describe Fisher–Kolmogorov type (or the so-called *pulled* [16]) fronts that correspond to the general one-variable equation

$$\partial u/\partial t = u - u^n + D_U \nabla^2 u, \quad n = 2 \text{ or } 3. \tag{48}$$

Such systems are characterized by a linear dependence of the reactive term $(u - u^n)$ on u in the vicinity of the steady state $u = 0$. In the vicinity of the SS, $h = 0$, $s = s_{in}$, where

$$E_S \cong K_S h \quad \text{and} \quad W_2 \cong 1 + s_{in} K_S. \tag{49}$$

Eq. (46) takes the form

$$\partial h/\partial t = (k_1 s_{in} K_S^2 h^3 + D_h \nabla^2 h)/(1 + s_{in} K_S). \tag{50}$$

So, the reaction term is proportional to h^3. Such fronts belong to the class of the so-called *pushed* fronts [16,17] that can emerge in bistable systems. The technique we used earlier for obtaining the speed of the front does not work for pushed fronts. Instead we can employ a technique used for equations of the following type

$$\partial h/\partial t = \varepsilon h + c_1 h^3 - c_2 h^5 + D_h \nabla^2 h \tag{51}$$

as $\varepsilon \to 0$ [17]. In our case

$$c_1 = k_1 s_{in} K_S^2/(1 + s_{in} K_S) \tag{52}$$

and c_2 can be calculated from the equality $c_2 = c_1/h_{SS}^2$, where $h_{SS} \cong s_{in}$. Hence,

$$c_2 = k_1 s_{in}^{-1} K_S^2/(1 + s_{in} K_S). \tag{53}$$

As shown by van Saarloos [17], the front velocity at $\varepsilon = 0$ can be expressed as

$$v = [D_h/(1 + s_{in} K_S)]^{1/2} c_1/(3c_2)^{1/2} \cong (k_1 s_{in} D_h/3)^{1/2}. \tag{54}$$

We have taken into account here that $1 \ll s_{in} K_S$. Eq. (54) implies that the velocity v is independent of K_S. We checked this conclusion by direct numerical integration of system (37)–(39) at very different K_S. We have found that at $k_1 = 10^4$ M^{-1} s^{-1}, $D_h = 2 \times 10^{-4}$ cm^2/s, and $s = 0.001$ M, the velocity v is almost independent of K_S (K_S was varied between 10^6 and 10^8 M^{-1}) and of D_S (varied from 0 to 10^{-5} cm^2/s) and is approximately equal to 3.2×10^{-3} cm/s, which is within 10%–20% of $(k_1 s_{in} D_h/2)^{1/2}$. Note the factor of 2 in the denominator, instead of 3 as in Eq. (54). This small difference may arise from the many simplifications in arriving at Eq. (54).

Another model. The autocatalytic reaction (32) can be written differently, namely as

$$s_1 + h \to 3h, \quad k_1. \tag{55}$$

In this case, the final reduced equations (analogous to (46), (47) at $D_S = 0$) are almost the same, with the exception that Eq. (46) should be replaced by

$$\partial h/\partial t = [k_1 s h E_S(1 + E_S) + D_h \nabla^2 h]/W_2. \tag{56}$$

Using the mass balance equation, $h + 2s_1 + s_0 = \text{constant} = s_{in}$, we can express s as

$$s = (s_{in} - h)/(E_S + 1)$$

and Eq. (56) can then be rewritten as

$$\partial h/\partial t = k_1 (s_{in} - h) h E_S/W_2 + D_h \nabla^2 h/W_2. \tag{57}$$

Let us introduce dimensionless variables $u = h/s_{in}$, $\tau = t k_1 s_{in}$, and $z = x(k_1 s_{in}/D_h)^{1/2}$. Then Eq. (57) becomes

$$\partial u/\partial \tau = u^2(1 - u)E_S'/W_2 + (1/W_2)\nabla^2 u \tag{58}$$

where $E_S' = K_S s_{in}/(1 + K_S s_{in} u)$. For the generic equation

$$\partial h/\partial \tau = a h^2(1 - h) + d\nabla^2 h, \tag{59}$$

which describes a pushed front in a bistable systems, the dimensionless front velocity is given by [13] $v = (da/2)^{1/2}$. If we return to dimensional variables, we have

$$v = (k_1 D_h/2K_S)^{1/2}. \tag{60}$$

Now, the front velocity is independent of s_{in}! We note that Eq. (60) holds only if $1 \ll s_{in} K_S$.

4. Simulations

A more detailed model. Now we consider a slightly more complex but still simple model, which is closer to our experimental system, since it incorporates the protonation of both the substrate s and the large molecule p. As before, only the protonated form of substrate, s_1, can participate in the autocatalytic reaction.

$$s_1 + h \to 2h \quad k_1, (\text{M}^{-1}\text{s}^{-1}) \tag{61}$$

$$s_0 + h \rightleftarrows s_1 \quad K_S, (\text{M}^{-1}) \tag{62}$$

$$p_0 + h \rightleftarrows p_1 \quad K_P, (\text{M}^{-1}). \tag{63}$$

Reactions (62) and (63) are very fast, limited by diffusion, and we assume that they are always at equilibrium. Eqs. (3) and (34) are still valid.

The reaction–diffusion equations for system (61)–(63) are

$$\partial h/\partial t = k_1 s_1 h + R_S + R_P + D_h \nabla^2 h \tag{64}$$

$$\partial s_1/\partial t = -k_1 s_1 h - R_S + D_S \nabla^2 s_1 \tag{65}$$

$$\partial s_0/\partial t = R_S + D_S \nabla^2 s_0 \tag{66}$$

$$\partial p_0/\partial t = R_P + D_P \nabla^2 p_0 \tag{67}$$

$$\partial p_1/\partial t = -R_P + D_P \nabla^2 p_1 \tag{68}$$

where $R_S = -k_d s_0 h + (k_d/K_S)s_1$ and $R_P = -k_d p_0 h + (k_d/K_P)p_1$ as before. We assign the same diffusion coefficient, D_S, to s_0 and s_1. To obtain a simpler system of equations, without the fast equilibrium reactions, we start from the following identity:

$$h + s_1 + p_1 = h + sE_S + pE_P. \tag{69}$$

Following the same procedure as before, we arrive at the final reduced set of equations:

$$\begin{aligned}\partial h/\partial t &= k_1 s h E_S^2/W_3 + D_h^* \nabla^2 h + H_S \nabla s \bullet \nabla h \\ &\quad + H_P \nabla p \bullet \nabla h + H_h \nabla h \bullet \nabla h\end{aligned} \tag{70}$$

$$\partial s/\partial t = -k_1 s E_S h + D_S \nabla^2 s \tag{71}$$

$$\partial p/\partial t = D_P \nabla^2 p \tag{72}$$

where

$$D_h^* = (D_h + D_S s G_S + D_P p G_P)/W_3 \tag{73}$$

$$W_3 = 1 + sG_S + pG_P \tag{74}$$

$$G_S = K_S/(1 + K_S h)^2, \qquad V_S = -2K_S^2/(1 + K_S h)^3 \tag{75}$$

$$G_P = K_P/(1 + K_P h)^2, \qquad V_P = -2K_P^2/(1 + K_P h)^3 \tag{76}$$

$$\begin{aligned}&H_S = 2D_S G_S/W_3, \qquad H_P = 2D_P G_P/W_3, \\ &\text{and} \quad H_h = (sD_S V_S + pD_P V_P)/W_3.\end{aligned} \tag{77}$$

Eqs. (70)–(72) constitute our reduced model. Note that if $D_P = 0$, the non-Fickian transport terms with H_S and H_h do not disappear. In addition to this difficulty, we would like to know how the front velocity depends on the initial pH, and therefore our initial state does not coincide with the steady state, where $h = 0$. In this case, introduction of the moving frame offers little help in finding an analytical expression for the front velocity. We have therefore undertaken extensive computer simulations of system (64)–(68) as well as system (70)–(72) to check that the latter system yields an accurate approximation to the full model.

The dependence of v on the large molecule concentration p is shown in Fig. 4. The calculated front velocities v for systems (64)–(68) and (70)–(72) are identical at the same parameters, verifying the assumption that equilibrium is rapidly established in Eqs. (62) and (63). We find that $1/v$ depends linearly on p as $1/v = cp + b$ with $c/b \cong K_p$ at any K_S and initial h_0. If we decrease h_0 by a factor of 10 (from 10^{-6} M to 10^{-7} M), then v decreases by the same factor at any p. If we increase K_S by a factor of 10 (from 10^6 to 10^7 M^{-1}) then v increases tenfold at any p. It thus appears that the front speed is proportional to the product $h_0 K_S$. Note that s_1 is proportional to $h_0 K_S$ at small h.

We also checked the dependence of v on K_p (Fig. 5a) and found that $1/v = cK_p + b$ with $c/b \cong p$. We suggest that, like the very simple model (1), (2) [see Eq. (30)], the expression for v contains a factor $(1 + pK_P)^{-1}$.

Varying k_1 by two orders of magnitude, we have found that $v \propto (k_1)^{0.6}$. The power 0.6 is unexpected, since theory predicts an exponent of 0.5. The dependence of v on s_{in} (Fig. 5b) is rather complex at small s_{in}, but above about $s_{in} = 0.004$ M, v can be approximated as $v \propto s_{in}$. This result is also unexpected, since in similar systems one usually finds $v \propto (s_{in})^{1/2}$.

We also studied the significance of the non-Fickian transport terms in Eq. (70). We simulated system (70)–(72) with only Fickian terms (with D_h^*, D_S, and D_P), taking $H_S = H_P = H_h = 0$, and found that v is significantly (2–3 times) larger than the value obtained with the full model at the same parameters (see Fig. 4). All non-Fickian terms are negative and reduce the front speed.

Diffusion. Eq. (70) demonstrates that protons have an effective Fickian diffusion coefficient D_h^* (Eq. (73)). If we remove the autocatalytic reaction (61) and leave only equilibrium reactions (62) and (63), then we can follow in a computer experiment how a small δ-function perturbation of h spreads in a one-dimensional system by recording the root mean square displacement of h, $\langle x_h^2 \rangle^{1/2}$:

$$\langle x_h^2 \rangle = \int_{-\infty}^{\infty} (x - x_0)^2 (h - h_0) \mathrm{d}x \Big/ \int_{-\infty}^{\infty} (h - h_0) \mathrm{d}x \tag{78}$$

where h_0 is the initial equilibrium concentration. We find that

$$\langle x_h^2 \rangle^{1/2} = 2D_h^* t. \tag{79}$$

If $p = s = 0$, then $\langle x_h^2 \rangle^{1/2} = 2D_h t$, as it should for normal or free diffusion of h in the absence of buffers.

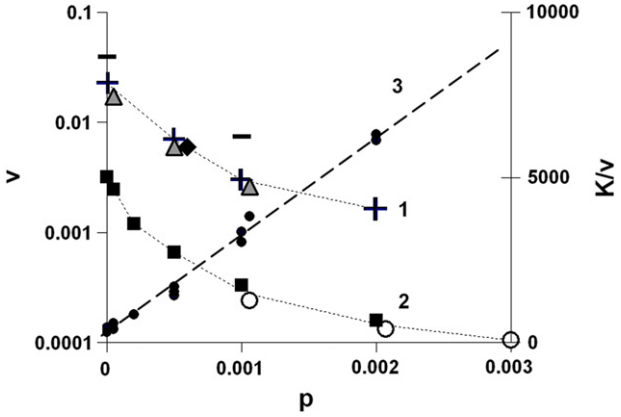

Fig. 4. Velocity of front propagation in model (61)–(63) as a function of p at $k_1 = 10^4$ M^{-1} s^{-1}, $s_{in} = s = 0.001$ M, $K_p = 10^4$ M^{-1}, $D_h = 2 \times 10^{-4}$ cm^2/s, $D_S = 1 \times 10^{-5}$ cm^2/s, $D_P = 1 \times 10^{-7}$ cm^2/s. Only small black dots and curve 3 (that fits these dots) belong to the right (K/v) axis. Curve 1, triangles, $h_0 = 10^{-7}$ M, $K_S = 10^7$ M^{-1}, pluses and single rhomb, $h_0 = 10^{-6}$ M, $K_S = 10^6$ M^{-1}; curve 2, squares and open circles; $h_0 = 10^{-7}$ M, $K_S = 10^6$ M^{-1}; pluses and open circles correspond to the results obtained from simulation of model (70)–(72), rhomb, triangles, and squares correspond to model (64)–(68); two dashes correspond to model (70)–(72) without non-Fickian terms at $h_0 = 10^{-6}$ M and $= 10^6$ M^{-1}. $K = 1$ and $K = 10$ for transformations of curves 2 and 1, respectively, into integrated curve 3 (K/v). Dependence K/v with $K = 1$ is fitted by straight line $1/v = cp + b$, with $c = 2.91 \times 10^6$ and $b = 2.83 \times 10^2$, $c/b \cong K_p$.

Model of the real BSFA system. Our full model for the BSFA system under batch conditions (without any inflow) consists of the following chemical reactions

$$3HSO_3^- + BrO_3^- \rightarrow 3H^+ + 3SO_4^{2-} + Br^-$$
$$r_1 = k_1[HSO_3^-][BrO_3^-] \tag{80}$$

$$3H_2SO_3 + BrO_3^- \rightarrow 6H^+ + 3SO_4^{2-} + Br^-$$
$$r_2 = k_2[H_2SO_3][BrO_3^-] \tag{81}$$

$$6HFe(CN)_6^{3-} + BrO_3^- \rightarrow 6Fe(CN)_6^{3-} + Br^- + 3H_2O$$
$$r_3 = k_3[HFe(CN)_6^{3-}][BrO_3^-] \tag{82}$$

$$6Fe(CN)_6^{4-} + BrO_3^- + 6H^+ \rightarrow 6Fe(CN)_6^{3-} + Br^- + 3H_2O$$
$$r_4 = k_4[Fe(CN)_6^{3-}][BrO_3^-] \tag{83}$$

$$Al(OH)_2^+ + H_2O \rightarrow Al(OH)_3(s) + H^+$$
$$r_5 = k_5[Al(OH)_2^+]\Theta \tag{84}$$

$$Al(OH)_3(s) + H^+ \rightarrow Al(OH)_2^+ + H_2O$$
$$r_6 = k_5 K_P[H^+]\Theta + k_6[H^+][Al(OH)_3(s)](1 - \Theta) \tag{85}$$

$$SO_3^{2-} + H^+ \rightleftarrows SO_3^- \quad K_{S1} \tag{86}$$

$$HSO_3^- + H^+ \rightleftarrows H_2SO_3 \quad K_{S2} \tag{87}$$

$$Fe(CN)_6^{4-} + H^+ \rightleftarrows HFe(CN)_6^{3-} \quad K_F \tag{88}$$

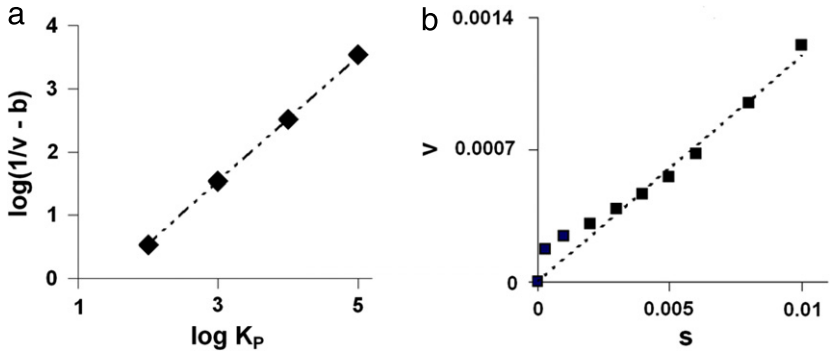

Fig. 5. (a) Front velocity v as a function of K_p in model (64)–(68). The linear dependence, $\log(1/v - b) = \log(K_p) - a$, shown in (a) with $b = 54$ and $a = 1.48$ is equivalent to $1/v = 10^{-a} \times K_p + b$. The ratio $10^{-a}/b$ is close to $p = 10^{-3}$; $s_{in} = 10^{-3}$. (b) Front velocity v as a function of substrate concentration s_{in} in model (64)–(68) at $K_P = 10^4$. For (a) and (b): $k_1 = 10^4\ \mathrm{M^{-1}s^{-1}}$, $K_S = 10^6\ \mathrm{M^{-1}}$, $k_d = 10^{10}\ \mathrm{M^{-1}s^{-1}}$, $D_h = 2 \times 10^{-4}\ \mathrm{cm^2/s}$, $D_S = 1 \times 10^{-5}\ \mathrm{cm^2/s}$, $D_P = 1 \times 10^{-7}\ \mathrm{cm^2/s}$, $p = 10^{-3}$ M, $h_0 = 10^{-7}$ M.

$$SO_4^{2-} + H^+ \rightleftarrows SO_4^- \quad K_{SA} \tag{89}$$

$$Al^{3+} + 2H_2O \rightleftarrows Al(OH)_2^+ + 2H^+ \quad K_A \tag{90}$$

where $k_1 = 4.9 \times 10^{-2}\ \mathrm{M^{-1}\ s^{-1}}$ (this work), $k_2 = 44\ \mathrm{M^{-1}\ s^{-1}}$ (this work), $k_3 = 8.5 \times 10^{-2}\ \mathrm{M^{-1}\ s^{-1}}$ [9], $k_4 = 5.5 \times 10^{-3}\ \mathrm{M^{-1}\ s^{-1}}$ (this work), $K_{S1} = 6.065 \times 10^6\ \mathrm{M^{-1}}$ ($\log K_{S1} = 6.78$), $K_{S2} = 58.74\ \mathrm{M^{-1}}$ ($\log K_{S2} = 1.77$) [19], $K_F = 12589\ \mathrm{M^{-1}}$ ($\log K_F = 4.10$) [20,21], $K_{SA} = 38.46\ \mathrm{M^{-1}}$ ($\log K_{SA} = 1.585$) [21]. Rate constants were determined by comparing the pH–time curves obtained from model simulations with those from our experiments in the stirred tank reactor. A large number of experiments run under different initial conditions allowed us to refine the values of k_1, k_2, and k_4 used in our previous paper [9] (namely $3.3 \times 10^{-2}\ \mathrm{M^{-1}\ s^{-1}}$, $22\ \mathrm{M^{-1}s^{-1}}$ and 0, respectively). The function Θ is defined as follows. If $[Al(OH)_2^+] > K_p[H^+]$, $\Theta = 1$. In this case, we assume that the precipitation–dissolution process is in quasi-equilibrium. Precipitate $Al(OH)_3(s)$ is formed with rate $k_5[Al(OH)_2^+]$ and dissolves with rate $k_5K_P[H^+]$. The ratio between these rates is the constant $K_P = 75.86$ ($\log K_P = 1.88$), which is obtained from the solubility product, $K_S = a_0/h^3 = 10^{11.01}\ \mathrm{M^{-2}}$, for amorphous $Al(OH)_3(s)$ [22,23] and the stability constant for $Al(OH)_2^+$, $K_A = 1.35 \times 10^9$ ($\log K_A = 9.13$) [23] ($K_P = K_S/K_A$). The value chosen for k_5 has little effect on the pH–time profiles and the front velocities. We take $k_5 = 10\ \mathrm{s^{-1}}$. If $[Al(OH)_2^+] < K_p[H^+]$, $\Theta =$ zero. In this case, only precipitate dissolution occurs. From literature data [24,25], we know that the dissolution rate in acidic conditions is proportional to the proton concentration and to $[Al(OH)_3(s)]^q$ where $q \in (2/3, 4/3)$. In our calculations, we use $k_6[H^+][Al(OH)_3(s)]$ for the precipitate dissolution rate. The value of k_6 is crucial for the existence of a minimum in the pH profile (Fig. 6a). We obtained $k_6 = 20\ \mathrm{s^{-1}}$ by fitting the batch experiments (*cf.* Fig. 1c, Fig. 6a).

The spatially extended system for front propagation in the BSFA system is described by the following PDEs:

$$\partial s_0/\partial t = -R_7 + D_{s0}\nabla^2 s_0 \tag{91}$$

$$\partial s_1/\partial t = R_7 - R_8 - 3r_1 + D_{s1}\nabla^2 s_1 \tag{92}$$

$$\partial s_2/\partial t = R_8 - 3r_2 + D_{s2}\nabla^2 s_2 \tag{93}$$

$$\partial f_0/\partial t = -R_9 - 6r_4 + D_{f0}\nabla^2 f_0 \tag{94}$$

$$\partial f_1/\partial t = R_9 - 6r_3 + D_{f1}\nabla^2 f_1 \tag{95}$$

$$\partial m_0/\partial t = -R_{10} + 3r_1 + 3r_2 + D_{m0}\nabla^2 m_0 \tag{96}$$

$$\partial m_1/\partial t = R_{10} + D_{m1}\nabla^2 m_1 \tag{97}$$

$$\partial b/\partial t = -r_1 - r_2 - r_3 - r_4 + D_b\nabla^2 b \tag{98}$$

$$\partial a_0/\partial t = -R_{11} + D_{a0}\nabla^2 a_0 \tag{99}$$

$$\partial a_2/\partial t = R_{11} - r_5 + r_6 + D_{a2}\nabla^2 a_2 \tag{100}$$

$$\partial a_3/\partial t = r_5 - r_6 \tag{101}$$

$$\partial h/\partial t = -R_7 - R_8 - R_9 - -R_{10} + 3r_1 + 6r_2 - 6r_4 + 2R_{11} + r_5 - r_6 + D_h\nabla^2 h \tag{102}$$

where $s_0 = [SO_3^{2-}]$, $s_1 = [HSO_3^-]$, $s_2 = [H_2SO_3]$, $b = [BrO_3^-]$, $f_0 = [Fe(CN)_6^{4-}]$, $m_1 = [HSO_4^-]$, $m_0 = [SO_4^-]$, $a_0 = [Al^{3+}]$, $a_2 = [Al(OH)_2^+]$ and $a_3 = [Al(OH)_3(s)]$; $R_7 = k_d(s_0h - s_1/K_{S1})$, $R_8 = k_d(s_1h - s_2/K_{S2})$, $R_9 = k_d(f_0h - f_1/K_F)$, $R_{10} = k_d(m_0h - m_1/K_{SA})$, $R_{11} = k_d(a_0 - a_2h^2K_A)$ and k_d is the diffusion-controlled reaction rate constant. Our measurements of ferricyanide and proton diffusion (Fig. 3b) in polyacrylamide gel show that their diffusion coefficients are close to those in aqueous solution. Hence, we use diffusion coefficients at infinite dilution in water solution at 25 °C for all species: $D_h = 9.3 \times 10^{-5}\ \mathrm{cm^2/s}$, $D_b = 1.5 \times 10^{-5}\ \mathrm{cm^2/s}$, $D_{f0} = 0.74 \times 10^{-5}\ \mathrm{cm^2/s}$ [26]. The diffusion coefficient of Na_2SO_3 is 1.258×10^{-5} for 0.075 M Na_2SO_3 [27]. We thus set $D_{s0} = 1.3 \times 10^{-5}\ \mathrm{cm^2/s}$, $D_{s1} = 1.3 \times 10^{-5}\ \mathrm{cm^2/s}$, $D_{s2} = 1.5 \times 10^{-5}\ \mathrm{cm^2/s}$, $D_{f1} = 0.9 \times 10^{-5}\ \mathrm{cm^2/s}$, $D_{a2} = 0.7 \times 10^{-5}\ \mathrm{cm^2/s}$ and $D_{a0} = 0.7 \times 10^{-5}\ \mathrm{cm^2/s}$. From our dynamic light scattering measurements we get a value of the order of $10^{-8}\ \mathrm{cm^2/s}$ for the diffusion coefficient of the precipitate. In our calculations, we set this parameter to zero.

We consider front propagation in the presence of precipitate in a one-dimensional finite closed system, $x \in [0, L]$ with $\nabla \equiv \partial/\partial x$ and $\partial/\partial x(x = 0) = \partial/\partial x(x = L) = 0$. The initial concentrations at $(t = 0, x)$ are the same as in the experiment in Fig. 1: $b = 0.065$ M, $s_0 = 0.075$ M, $s_1 = s_2 = 0$, $f_0 = 0.015$ M, $f_1 = 0$, $a_0 = a_2 = 0$, and $a_3 = a_{in}$. A small perturbation: h (at $t = 0, x < L_p$) $= 0.06$ M and h ($t = 0, x > L_p$) $= 0.02$ M where $L_p \ll L$, is introduced to initiate the front.

The front velocities v are measured at the inflection points, where the velocities have their minimum values, in the curves shown in Fig. 7a. The dependence of v on a_{in} (total amount of aluminum added) is shown in Fig. 7b. The dependence of $1/v$ on a_{in} is almost linear: $1/v = 1/v_0 + ca_{in}$, $c = 328\ \mathrm{min/(mm \times M)}$, if we ignore the last point at $a_{in} = 0.04$ M. At large a_{in}, the time needed to reach the true minimum velocity (the theoretical minimum) may be longer than the induction time for global autocatalysis, and therefore our measured value of v may exceed the expected value. The model (91–102) describes the experimental system quite well. It gives pH–time curves similar to those observed in the stirred tank reactor (*cf.* Figs. 1 and 6a). It also reproduces the patterns of fronts observed in the polyacrylamide gel experiments (Figs. 1 and 6b) and the decrease of the front velocity with increasing total aluminum concentration a_{in}.

In the models presented in Section 3 we assume that solubility of the precipitate [$p_0 = p/(1 + K_ph)$, Eq. (2)] is proportional to total concentration of aluminum, p. However, in precipitation

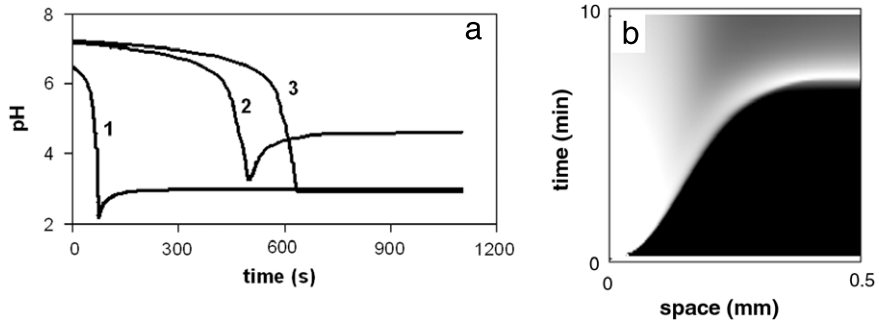

Fig. 6. (a) pH profile for $a_{in} = 0.01$ M in batch system. (b) Space–time plot for $a_{in} = 0.005$ M. Grayscale changes from white (pH < 3) through gray (pH 4.6) to black (pH > 5).

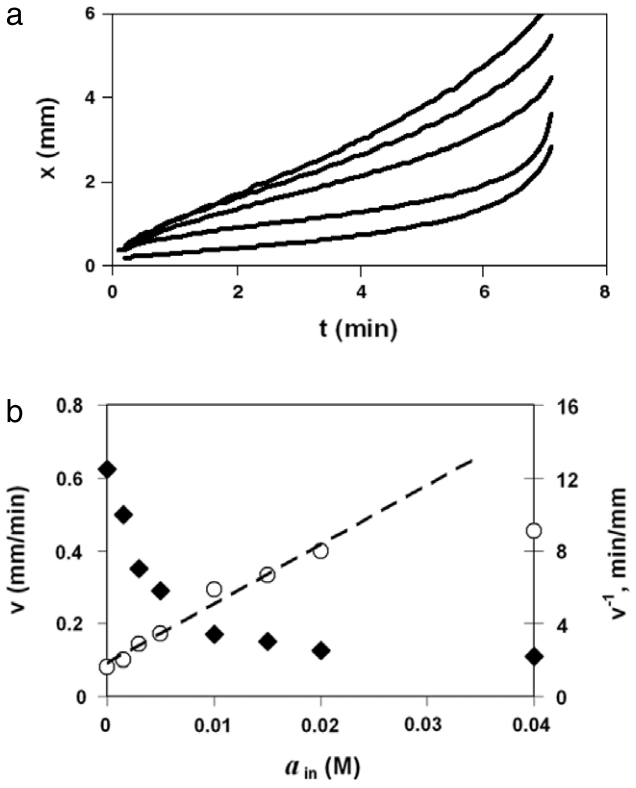

Fig. 7. (a) Front coordinate (at pH 4.6) as a function of time for the total concentrations of aluminum $a_{in} = 0$, 0.0015 M, 0.003 M, 0.01 M, and 0.04 M (from top to bottom). (b) Dependence of the minimum front velocity in the BSFA model on the total concentration of aluminum.

equilibrium, the concentrations of soluble forms of aluminum in the solution above the precipitate (solubility) depend only on the pH. In this section, we study such a situation. In the model (91)–(102), the solubility is equal to

$$a = a_0 + a_2 = K_p h(1 + K_A h^2) \tag{103}$$

if we consider Eqs. (84), (85) and (90) as fast equilibria. For the model (91)–(102) we can derive a result similar to Eq. (20):

$$\begin{aligned}\partial h/\partial t = {} & [3(r_1 + r_2)(E_s - E_m) - 6(r_3 + r_4)(1 - E_f) \\ & + (3 + 2E_a)(r_5 - r_6)]/W \\ & + [(D_h + G_s s D_s + G_f f D_f + G_m m D_m + 2G_a a D_a)/W]\nabla^2 h \\ & + D_S[V_s s(\nabla h)^2 + 2G_s \nabla s \bullet \nabla h]/W \\ & + D_f[V_f f(\nabla h)^2 + 2G_f \nabla f \bullet \nabla h]/W \\ & + D_m[V_m m(\nabla h)^2 + 2G_m \nabla m \bullet \nabla h]/W \\ & + 2D_a[V_a a(\nabla h)^2 + 2G_a \nabla a \bullet \nabla h]/W \end{aligned} \tag{104}$$

where

$$\begin{aligned} & s = s_0 + s_1 + s_2, \qquad f = f_0 + f_1, \qquad m = m_0 + m_1, \\ & E_s = (K_{S1}h + 2K_{S1}K_{S2}h^2)/(1 + K_{S1}h + K_{S1}K_{S2}h^2), \\ & E_f = K_F h/(1 + K_F h), \qquad E_m = K_{SA}h/(1 + K_{SA}h), \\ & E_a = -1/(h^2 K_A + 1), \qquad W = 1 + G_s s + G_f f + G_m m + 2G_a a, \\ & G_s = \mathrm{d}E_s/\mathrm{d}h \\ & \quad = K_{S1}(K_{S1}K_{S2}h^2 + 4K_{S2}h + 1)/(1 + K_{S1}h + K_{S1}K_{S2}h^2)^2, \\ & G_f = K_F/(1 + K_F h)^2, \qquad G_m = K_{SA}/(1 + K_{SA}h)^2, \\ & G_a = 2K_A h/(1 + K_A h^2)^2, \\ & V_s = \mathrm{d}^2E_s/\mathrm{d}h^2 = -2K_{S1}(K_{S1}^2K_{S2}^2h^3 + 6K_{S1}K_{S2}^2h^2 \\ & \quad + 3K_{S1}K_{S2}h + K_{S1} - 2K_{S2})/(1 + K_{S1}h + K_{S1}K_{S2}h^2)^3, \\ & V_f = -2K_F^2/(1 + K_F h)^3, \qquad V_m = -2K_{SA}^2/(1 + K_{SA}h)^3, \\ & V_a = -2K_A(3h^2K_A - 1)/(h^2K_A + 1)^3. \end{aligned}$$

In deriving Eq. (104) we assume that $D_{s0} = D_{s1} = D_{s2} = D_s$, $D_{f0} = D_{f1} = D_f$, $D_{m0} = D_{m1} = D_m$, $D_{a0} = D_{a2} = D_a$. We see that the Fickian term

$$D_h^* = (D_h + G_s s D_s + G_f f D_f + G_m m D_m + 2G_a a D_a)/W \tag{105}$$

depends on a, but a does not depend on $a_{in} = a + a_3$ (see Eq. (103)). Nevertheless, the front velocity decreases when a_{in} is increased (Fig. 7b). We conclude that this decrease results from the slow dissolution of precipitate below pH = 4.34 (for $a_{in} = 0.01$ M), the second term in the rate expression of Eq. (85). This precipitate dissolution is an additional factor that can decrease the front velocity, especially at lower a_{in}, when nearly all the precipitate is dissolved behind the front. This effect constitutes a significant difference between polymer buffer systems (such as poly(acrylate) or poly(vinyl alcohol)) and precipitation systems like the one considered here.

As we did for Eq. (70), we can analyze the non-Fickian terms in Eq. (104). The terms G_s, G_f, G_m and G_A are positive for all h. Hence, the terms $2G_s \nabla s \bullet \nabla h$ and $2G_f \nabla f \bullet \nabla h$ are negative (because the gradients of h and of s and f point in opposite directions) and therefore decrease the front velocity. The term $2G_m \nabla m \bullet \nabla h$ is positive and increases the front velocity, but it is small at the leading edge of the front, and it is important only at low pH and when m is large, i.e., behind the front. Finally, $2G_a \nabla a \bullet \nabla h$ is positive and makes a positive contribution to the front velocity. Because V_s, V_f, and V_m are negative for all h, the terms $V_s s(\nabla h)^2$, $V_f f(\nabla h)^2$, and $V_m m(\nabla h)^2$ are negative and retard the front. V_a is positive for $h^2 < 1/(3K_A)$ and changes sign above this value. At $h^2 = 1/K_A$ (pH = 4.56) V_a is minimum; it approaches zero for large proton concentrations. Hence, the equilibrium (90) decreases the front velocity for $h^2 > 1/(3K_A)$ (pH < 4.80).

5. Discussion

We have investigated front propagation in a buffered system in which H^+ is the autocatalytic species from three points of view: experimental, theoretical, and numerical simulations. We now attempt to bring these results together. Our experiments show that the speed of front propagation decreases with the concentration of $Al(OH)_3$, which acts as a buffer for protons. However, $Al(OH)_3$ is not a simple buffer, since the slow dissolution of precipitate and possible surface reactions may affect the kinetics of the system. Nonetheless, we have treated it as a simple buffer to simplify our models while maintaining the overall effect of $Al(OH)_3$ on the dynamics of the system. The theoretical analysis demonstrates that our front is a *pulled* front rather than a *pushed* one, due to protonation of the substrate sulfite (reactions 86 and 87), despite the fact that this front links an unstable initial state to the stable final steady state. In addition, our initial state is not the steady state, which further complicates the theoretical analysis. As a result of this complexity we have, for example, a strong dependence of the front velocity on the initial h_0 and the expected dependence of the front velocity on the initial substrate concentration, $v \propto (s_{in})^{1/2}$, is replaced by $v \propto s_{in}$ (see Fig. 5b).

We have focused on the dependence of v on the concentration of buffer (a_{in}, the total concentration of all protonated and deprotonated forms of Al, or p in the simpler model 1–3). The experiment (Fig. 3) points out that this dependence arises from a decrease in the effective diffusion coefficient D_h^* of protons, which can be expressed by Eq. (73) as $D_h^* \propto A_1/(A_2 + A_3 p)$ (when $D_p \cong 0$, the variable p in model (61)–(63) plays the same role as a_{in} in model (80)–(90)), where A_1, A_2, and A_3 are constants. If we assume the usual dependence of v on D, as $v \propto (D_h^*)^{1/2}$, we reach the incorrect conclusion that $v^{-1} \propto (A_2 + A_3 p)^{1/2}$. The experiments (Fig. 2), our simple theoretical analysis Eq. (30), and the more complex simulations (Fig. 4 and Fig. 7b) all agree that

$$v^{-1} \propto v_0^{-1} + c a_{in} \tag{106}$$

where the constant c depends on the protonation constant K_P, $(D_h)^{-1/2}$, and some other parameters. The dependence of the front velocity in the chlorite–tetrathionate reaction on the concentration of immobile COO^- groups of methacrylate, c_M (c_M is analogous to a_{in}) [15] also obeys Eq. (106) (as we can recalculate from the dependence shown in Fig. 4 of Ref. [15]), if c_M is smaller than some critical value at which the front instability starts. Since the rate of autocatalysis in the chlorite–tetrathionate reaction is proportional to $[H^+]^2$, while in our case the rate of autocatalysis is proportional to $[H^+]$ for model (1)–(2) and to $[H^+]^3$ for model (32) and (33) (see Eq. (50)), we suggest that relation (106) may apply to any type of autocatalysis.

In our full model (80)–(90), the protonation with equilibrium constant K_P and the slow dissolution of precipitate a_3 with rate constant k_6 both affect the front velocity and contribute to the expression (106).

The full model (91)–(102) can be reduced to a much simpler model like Eqs. (70)–(72), where all fast equilibrium reactions are eliminated and Fickian (e.g., $D_h^* \nabla^2 h$) and non-Fickian (e.g., $H_S \nabla s \bullet \nabla h$) transport terms are introduced. Analogous non-Fickian terms were obtained in the case of diffusion of free Ca^{2+} in a buffered medium [6]. These non-Fickian terms significantly reduce the speed of the front and contribute to the dependence (106).

The dependence of D_h^* on the buffer concentration p Eq. (73) shows that D_h^* can be quite small at high p, if D_p, the diffusion coefficient of the buffer molecules, is very small. In systems like the FIS reaction [1–5], such a small D_h^* may give rise to Turing patterns.

Acknowledgement

This work was supported by the National Science Foundation through grant CHE-0615507.

References

[1] K.J. Lee, W.D. McCormick, Q. Ouyang, H.L. Swinney, Pattern-formation by interacting chemical fronts, Science 261 (1993) 192–194.
[2] K.J. Lee, W.D. McCormick, J.E. Pearson, H.L. Swinney, Experimental observation of self-replicating spots in a reaction-diffusion systems, Nature 369 (1994) 215–218.
[3] K.J. Lee, H.L. Swinney, Lamellar structures and self-replicating spots in a reaction-diffusion system, Phys. Rev. E 51 (1995) 1899–1915.
[4] K.J. Lee, H.L. Swinney, Replicating spots in reaction-diffusion systems, Internat. J. Bifur. Chaos 7 (1997) 1149–1158.
[5] I. Szálai, P. De Kepper, Pattern formation in the ferrocyanide-iodate-sulfite reaction: The control of space scale separation, Chaos 18 (2008) 026105.
[6] J. Wagner, J. Keizer, Effects of rapid buffers on Ca^{2+} diffusion and Ca^{2+} oscillations, Biophys. J. 67 (1994) 447–456.
[7] E.C. Edblom, et al., Kinetics and mechanism of the oscillatory bromate sulfite ferrocyanide reaction, J. Phys. Chem. 93 (1989) 2722–2727.
[8] K. Kurin-Csörgei, I.R. Epstein, M. Orbán, Systematic design of chemical oscillators using complexation and precipitation equilibria, Nature 433 (2005) 139–142.
[9] K. Kovacs, M. Leda, V.K. Vanag, I.R. Epstein, Small amplitude and mixed mode pH oscillations in the bromate–sulfite–ferrocyanide–aluminum(III) system, J. Phys. Chem. A 113 (2009) 146–156.
[10] Z. Virányi, I. Szálai, J. Boissonade, P. De Kepper, Sustained spatiotemporal patterns in the bromate-sulfite reaction, J. Phys. Chem. A 111 (2007) 8090–8094.
[11] A. Keresztessy, I.P. Nagy, G. Bazsa, J.A. Pojman, Traveling waves in the iodate-sulfite and bromate-sulfite systems, J. Phys. Chem. 99 (1995) 5379–5384.
[12] D.G. Míguez, V.K. Vanag, I.R. Epstein, Fronts and pulses in an enzymatic reaction catalyzed by glucose oxidase, Proc. Natl. Acad. Sci. 104 (2007) 6992–6997.
[13] P. Gray, S.K. Scott, Chemical Oscillations and Instabilities: Non-linear Chemical Kinetics, Vol. 21, Clarendon Press, Oxford University Press, Oxford, 1990.
[14] I. Lengyel, I.R. Epstein, A chemical approach to designing turing patterns in reaction-diffusion systems, Proc. Natl. Acad. Sci. 89 (1992) 3977–3979.
[15] D. Horváth, A. Tóth, Diffusion-driven front instabilities in the chlorite-tetrathionate reaction, J. Chem. Phys. 108 (1998) 1447–1451.
[16] W. van Saarloos, Front propagation into unstable states: Marginal stability as a dynamical mechanism for velocity selection, Phys. Rev. A 37 (1988) 211–229.
[17] W. van Saarloos, Front propagation into unstable states. II. Linear versus nonlinear marginal stability and rate of convergence, Phys. Rev. A 39 (1989) 6367–6390.
[18] W. van Saarloos, Front propagation into unstable states, Phys. Rep. 386 (2003) 29–222.
[19] T.G. Szanto, G. Rábai, pH oscillations in the BrO3(-)–SO32–/HSO3- reaction in a CSTR, J. Phys. Chem. A 109 (2005) 5398–5402.
[20] J. Jordan, G.J. Ewing, Protonation of hexacyanoferrates, Inorg. Chem. 1 (1962) 587–691.
[21] J. Zagora, M. Voslar, L. Schreiberova, I. Schreiber, Excitable dynamics in the bromate-sulfite-ferrocyanide reaction, Phys. Chem. Chem. Phys. 4 (2002) 1284–1291.
[22] M. Dietzel, G. Bohme, The dissolution rates of gibbsite in the presence of chloride, nitrate, silica, sulfate, and citrate in open and closed systems at 20 degrees C, Geochim. Cosmochim. Acta 69 (2005) 1199–1211.
[23] J.Y. Bottero, J.M. Cases, F. Fiessinger, J.E. Poirier, Studies of hydrolyzed aluminum-chloride solutions. 1. Nature of aluminum species and composition of aqueous-solutions, J. Phys. Chem. 84 (1980) 2933–2939.
[24] A. Packter, H.S. Dhillon, Heterogeneous reaction of gibbsite powder with aqueous inorganic acid solutions — Kinetics and mechanism, J. Chem. Soc. A (1969) 2588–2593.
[25] E.Y. Nevskaya, et al., alpha-Al(OH)(3) dissolution in acid media, Theor. Found. Chem. Eng. 34 (2000) 292–297.
[26] J.S. Newman, Electrochemical Systems, Prentice Hall, Englewood Cliffs, 1973.
[27] D.G. Leaist, Moments analysis of restricted ternary diffusion — Sodium sulfite+sodium hydroxide+water, Can. J. Chem. 63 (1985) 2933–2939.